Detection of the tagged or untagged photons in acousto-optic imaging of thick highly scattering media by photorefractive adaptive holography

Michel Gross, Max Max Lesaffre, François Ramaz, Philippe Delaye, Gérald Roosen, Claude Boccara

Eur. Phys. J. E **28**, 173–182 (2009)
DOI 10.1140/epje/i2008-10408-2

THE EUROPEAN PHYSICAL JOURNAL E

Regular Article

Detection of the tagged or untagged photons in acousto-optic imaging of thick highly scattering media by photorefractive adaptive holography

M. Gross[1], M. Lesaffre[1,2], F. Ramaz[2,a], P. Delaye[3], G. Roosen[3], and A.C. Boccara[2]

[1] Laboratoire Kastler-Brossel, UMR 8552 (ENS, CNRS, UMPC), Ecole Normale Supérieure, 10 rue Lhomond, 75231 Paris cedex 05, France
[2] Laboratoire d'Optique, Ecole Supérieure de Physique et de Chimie Industrielles de la Ville de Paris, CNRS UPRA0005, Université Pierre et Marie Curie, 10 rue Vauquelin, 75231 Paris cedex 05, France
[3] Laboratoire Charles Fabry de l'Institut d'Optique, CNRS, Université Paris-Sud, Campus Polytechnique, RD128, 91127 Palaiseau cedex, France

Received 27 May 2008 and Received in final form 10 September 2008
Published online: 22 December 2008 –

Abstract. We propose an original adaptive wavefront holographic setup based on the photorefractive effect (PR), to make real-time measurements of acousto-optic signals in thick scattering media, with a high flux collection at high rates for breast tumor detection. We describe here our present state of the art and understanding on the problem of breast imaging with PR detection of the acousto-optic signal.

PACS. 42.25.Dd Wave propagation in random media – 42.30.Ms Speckle and moiré patterns – 42.40.Ht Hologram recording and readout methods – 42.70.Ln Holographic recording materials; optical storage media

1 Introduction

The field of acousto-optic imaging has been strongly stimulated by the deep and complete paper of W. Leutz and G. Maret [1]. In this paper the authors give a very clear view of the tricky interactions between light and sound in random media; this is why this work has stimulated a new active field now more "biomedical imaging" oriented and new detection schemes.

The present paper is at the frontier of two physical domains that are

i) detection of weak light signal by using photorefractive crystals,
ii) breast cancer imaging by detection of the ultrasonic modulation of the light scattered through the breast.

Here, our purpose is to make a brief review of these two domains, and to describe the photorefractive detection of the scattered-light modulated component in a pedagogical manner. By the way, we will describe our present state of the art and understanding on the problem.

In this paper, we will first describe the basic principle of ultrasonic modulation of light imaging. We will, in particular, introduce the concept of "ultrasonic tagged photons", which represents the weak signal to be detected. We will then describe how photorefractive adaptive holography can be used to detect the tagged photons. One must notice that all the groups working on the subject, except for us, do not detect the "tagged" photons, but the "untagged" ones. The tagged-photon signal is measured indirectly, since the total number of scattered photons (tagged + untagged) does not depend on the ultrasound. We will describe our technique and present our experimental results. In all these descriptions, we must not forget one difficulty that results from the decorrelation of the light that travels through the breast organ. This effect known as speckle decorrelation is both due to the Brownian motion of the scatterers, and to the breast inner motions (blood flow, ...). In a typical in vivo situation, with 4 cm breast thickness, the "speckle decorrelation time" is in the 0.1 to 1 ms range. It is thus necessary to match the so called "photorefractive response time" with the "speckle decorrelation time". This effect, which is huge in breast, is not present in most of the ultrasonic modulation test experiments, which are performed with breast phantoms like dead tissues or diffusing gels. Since the decorrelation affects considerably the detection sensitivity, it is quite difficult to evaluate the figure of merit of the different techniques that are proposed to perform breast imaging. We will see that our setup, which is able

[a] e-mail: ramaz@optique.espci.fr

to detect both the tagged and untagged signal, is also able to measure the photorefractive time *in situ, i.e.* with the same setup, same laser powers and same sample geometry as for breast imaging experiments. To our knowledge, nobody is presently able to perform ultrasonic modulation imaging through 4 cm of breast tissues *in vivo*. Experiments are under progress and we hope to be able to reach this aim in a near future.

2 Acousto-optic imaging

The combination of light and ultrasound to measure local optical properties through thick and highly scattering media is a tantalizing approach for *in vivo* imaging. It is an alternative solution to pure optical techniques for breast cancer detection. The use of light is motivated by its relative low absorption in the so-called "optical therapeutic window" (700 nm to 1000 nm), and by the existence of optical contrasts between healthy and tumorous areas in this region of the spectrum.

Light is highly scattered within biological tissues, making direct optical study of thick sample very difficult to perform. Light scattering is characterized by two length parameters, *i.e.* the scattering length l_s, and the light transport mean free path l_s^*. The scattering length l_s characterizes the memory of the optical phase, and corresponds to the average distance that separates two scattering events. The light transport mean free path l_s^* characterizes the memory of the light propagation direction. In tissues, l_s is typically 50 to 100 μm, while l_s^* is 10 times larger (0.5 to 1 mm). Absorption of light is characterized by the absorption length l_a, which is in the 1 cm to 10 cm range. Absorption strongly depends on the nature of the tissue (optical contrast).

Because of scattering, direct imaging cannot be performed through more than a few millimeter thick samples. Contrarily to light, ultrasound (US) beams are ballistic in biological tissues. US gives thus access to millimeter range spatial resolution in thick sample (up to 4 cm) yielding the development of the acousto-optic imaging that combines optics and ultrasound [2,3].

2.1 Principle: the tagged photons

Acousto-optic imaging is a hybrid technique, which combines, thanks to the acousto-optic effect, ultrasound and light. US are applied in the region of interest, within the thick scattering sample (see Fig. 1a). They make the scatterers vibrate. A CW laser (frequency ω_L) illuminates the sample. The vibration of the scatterers at the acoustic US frequency ω_A (2 MHz typically) modulates the phase of the photons that are scattered by the sample. This is the so-called acousto-optic effect.

The light exiting the sample contains thus different frequency components (see Fig. 1b). The main component (the carrier) is centered at the laser frequency ω_L. It is related to the diffused photons, that do not interact with the US. The sideband components are shifted by the US frequency $\omega_L \pm \omega_A$. The sideband photons, which result from the interaction between light and US, are called "tagged photons" (*i.e.* photons tagged by the US).

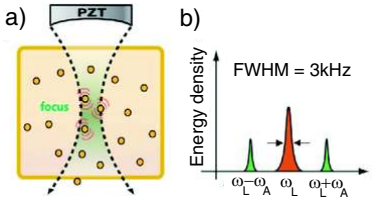

Fig. 1. Principle of acousto-optic imaging. a) Motion of the scatterer at ω_A. b) Spectrum of the diffused light: carrier (ω_L), and sideband, *i.e.* tagged photons ($\omega_L \pm \omega_A$).

The weight of the tagged-photons components depends on the optical absorption in the region of interest, where the US beam is focused. Acousto-optics imaging stands in detecting selectively the tagged photons. An image of the sample optical absorption can be then built up in scanning the US over the sample. Note that one of the difficulties in living tissues results from the motion of scatterers (*e.g.* blood flow) which broaden the carrier and sideband lines (see Fig. 1b). *In vivo* measurements through 4 cm breast tissues yield a broadening of 1.5 kHz (Full Width at Half Maximum: FWHM) [4,5].

2.2 State of the art for the detection of the tagged photons

Many techniques have been proposed to detect the tagged photons. Marks *et al.* [6] investigated the modulation of light in homogeneous scattering media with pulsed ultrasound. Wang *et al.* [2,7] performed ultrasound modulated optical tomography in scattering media. Lev *et al.* studied scattering media in the reflection configuration [8]. Wang and Shen [9] developed a frequency chirp technique to obtain scalable imaging resolution along the ultrasonic axis by use of a one-dimensional (1D) Fourier transform. Lev *et al.* use a set of optical fibers coupled to a single photo-detector [5, 8, 10] that allows to work with samples, which decorrelate in time. Leveque *et al.* [11–13] performed parallel detection of multiple speckles on a video camera and demonstrated improvement of the detection signal-to-noise ratio of 1D images of biological tissues. The parallel detection has been still improved by Gross *et al.*, who perform holographic detection reaching the shot noise sensitivity limit [14], and by Atlan *et al.*, who get resolution on the US propagation axis by using a holographic pulsed technique [15].

All these methods exhibit two main limitations. First, the *optical etendue* (defined as the product of the detector area by the detector acceptance solid angle) of the detection system is not optimum, since it is much lower than the *etendue* of the tagged photons source. This *etendue* is the area of the sample (several cm^2) $\times$ the emitting solid angle (which is about 2π, since the light is diffused by the sample in all directions). With a mono detector (photodiode) [5, 8, 10] the detection *etendue* is about λ^2. With a

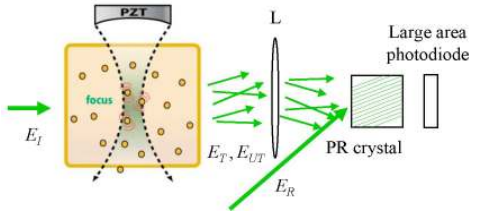

Fig. 2. Principle of PR detection of the acousto-optic signal. PZT: ultrasound transductor, E_I: illumination optical field; E_T, E_{UT}: tagged or untagged field scattered by the sample; PR crystal: photorefractive crystal; L: lens that collects the scattered field into the crystal and the photodiode; E_R: PR crystal reference (or pump) field.

multi-detector like a CCD camera [11–15] the *etendue* is $N\lambda^2$, where N is the is CCD number of pixel ($N \sim 10^6$). Even with a camera, the *etendue* of detection is about $\times 1000$ lower than the *etendue* of the emission.

The second problem occurs within living sample: the scatterers move, yielding in the frequency space a broadening of the tagged photons spectrum, as shown in Figure 1b [4, 5]. This effect corresponds, in the time space, to a decorrelation of the tagged-photons speckle pattern. Since all the methods described above perform coherent detection, the bandwidth of detection is limited by the detector bandwidth. With a camera (there is no problem of bandwidth with the photodiode, but the *etendue* is much lower), the bandwidth is roughly equal to the camera image frequency ω_{CCD}, which is in general much lower ($\omega_{CCD} \sim 10$–$100\,\mathrm{Hz}$) than the tissue broadening ($3\,\mathrm{kHz}$). It is still possible to work with fast camera (kHz), but in that case: i) the camera quantum efficiency is lower (CMOS), and ii) the number of pixel N is limited, because $N \times \omega_{CCD}$ is the flux of information to transfer to the computer, and this flux is limited ($< 10^6$–$10^7\,\mathrm{s}^{-1}$).

3 The photorefractive (PR) detection of the acousto-optic signal

More recently a new tagged-photons detection technique has appeared that is based on the photorefractive effect (PR) and that is illustrated by Figure 2. The light that is scattered by the sample (E_T or E_{UT} for the tagged or untagged field) is detected by a photorefractive detector (PR crystal + photodiode PD) that is pumped by a reference field E_R.

Since the crystal and the photodiode might be quite large (up to $1\,\mathrm{cm}^2$) and since the light is collected by a large Numerical Aperture (N.A. ~ 1) collecting lens, the photorefractive detection benefits of a high *etendue*, about 100 times larger than in a typical camera with $N \sim 10^6$ pixels. We will see that the detection bandwidth is the inverse of the "photorefractive time" T_{PR}. We get, for example, for a $1\,\mathrm{W/cm}^2$ pump beam, $1/T_{PR} \sim 1\,\mathrm{kHz}$ [16, 17]. This bandwidth, which is about 100 times larger than

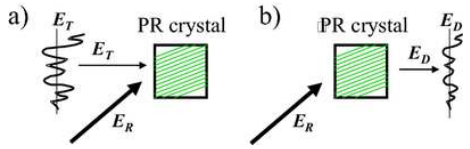

Fig. 3. Principle of holography using the photorefractive effect.

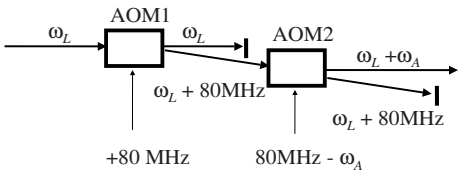

Fig. 4. Method for tuning the frequency ω_R of the reference beam: $\omega_R = \omega_L + \omega_A$ for example. AOM1 and AOM2 are acousto-optic modulators.

for a $N \sim 10^6$ CCD camera[1], is within the range of the linewidth ($\sim 3\,\mathrm{kHz}$) of the light scattered *in vivo* by a breast organ [4].

3.1 The volume hologram

Photorefractive effect arises in materials that present both electro-optic effect and photoconductivity, whose combination allows to transform a non-uniform illumination of the material into a spatial variation of the refractive index [18]. When illuminated by the interference pattern between an object and a reference beam, the material records a hologram, *i.e.* the amplitude and phase of the object beam. This hologram is dynamic, meaning that it can follow the interference pattern fluctuations slower than the response time T_{PR} of the material, also meaning that only slowly moving holograms are recorded.

The first effect is the recording of the signal beam information (phase and amplitude of the signal field E_T) within the PR crystal under the form of local changes of the crystal refractive index n yielding a volume hologram (Fig. 3a). Since the recording takes a finite time T_{PR} (0.1 to 10 ms in our device), the PR effect selects, within the signal beam, the components whose frequency is close or equal to the reference beam frequency ω_R.

Here, the large, almost flat field, reference beam (field E_R) interferes with the signal field E_T onto the PR crystal. In order to select the tagged or untagged photons, the frequency ω_R of the reference beam is made equal to the tagged or untagged photons frequency: $\omega_R = \omega_L \pm \omega_A$ or $\omega_R = \omega_L$, respectively. To adjust ω_R one can use, for example, two acousto-optic modulators AOM1 and AOM2 (Bragg cells) as shown in Figure 4. With such a choice, the interference pattern $E_T E_R^*$ of the reference beam with the selected photons beam varies slowly in time. The selected beam information can thus be grooved within the PR crystal volume hologram.

[1] We implicitly exclude here fast CMOS camera because of poor quantum efficiency and noise, and because of finite bandwidth for the data transfert form camera to computer.

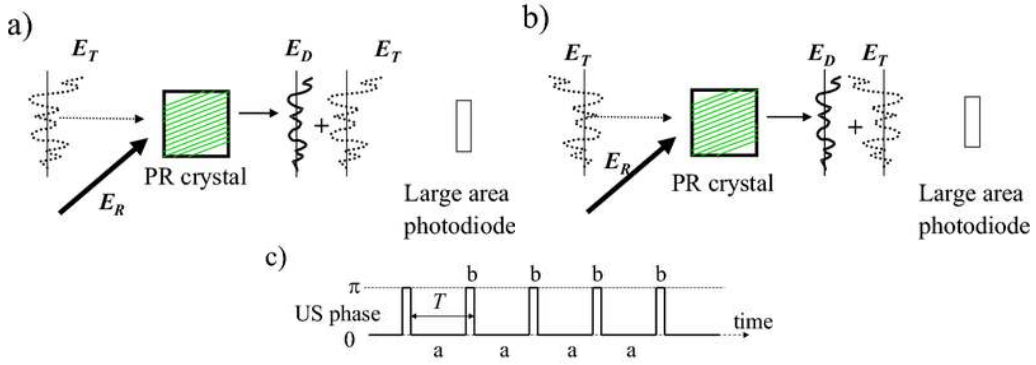

Fig. 5. Detection of the tagged photons, when the phase of the US beam is zero (a) and π (b). c) Phase of the US beam.

In the case of a perfect monochromatic signal beam, the local variation of the hologram refractive index δn is simply proportional to the modulation depth of the interference pattern $(E_T E_R^*)/(|E_T|^2 + |E_R|^2)$. If a time modulation is added on the signal (*e.g.* amplitude or phase modulation), we have to take into account the finite time T_{PR} needed to groove the hologram, and we get [19,20]

$$\delta n \propto \frac{\langle E_T E_R^* \rangle_{T_{PR}}}{|E_T|^2 + |E_R|^2}\,, \tag{1}$$

where $\langle\ \rangle_{T_{PR}}$ is the average over the grooving time T_{PR}, average which is defined by

$$\langle A \rangle_{T_{PR}} = \frac{1}{T_{PR}} \int_0^\infty A(t-\tau)\, e^{-\tau/T_{PR}} \mathrm{d}\tau. \tag{2}$$

3.2 The diffracted beam E_D

The second effect is illustrated by Figure 3b. The reference beam (E_R) is diffracted by the volume hologram yielding a diffracted beam (E_D). The diffracted field E_D is simply proportional to the hologram refractive-index changes δn and to the reference beam field E_R. We get thus

$$E_D \propto \frac{\langle E_T E_R^* \rangle_{T_{PR}}}{|E_T|^2 + |E_R|^2} E_R. \tag{3}$$

In a typical application the reference beam intensity is much larger than the signal beam one, and except of the average over T_{PR}, E_R and E_R^* simplifies in equation (3) yielding $E_D \propto E_T$, *i.e.*

$$E_D \simeq \eta E_T, \tag{4}$$

where $\eta = 0.1, \ldots, 0.5$ is a numerical factor which mainly depends on the crystal.

Equation (4) is valid, when the decorrelation of the signal field E_T can be neglected during the grooving time T_{PR}, *i.e.* when

$$\delta\omega T_{PR} \ll 1, \tag{5}$$

where $\delta\omega$ is the frequency width of the signal beam ($\Delta\omega \sim 3\,\mathrm{kHz}$ for the breast).

We have to notice that an increase of the reference beam intensity $|E_R|^2$ does not change η, but reduces the grooving time T_{PR}, since $T_{PR} \propto 1/|E_R|^2$. The main advantage of increasing the reference beam power $|E_R|^2$ is thus to reduce T_{PR} enough to neglect the signal field decorrelation. Condition of equation (5) is then fulfilled, and the equation (4) limit can be reached.

Since the volume hologram has recorded the mode structure of the signal beam *versus* the reference beam interference pattern, and since the pump beam is diffracted by the hologram, the diffracted beam (E_D) has the same mode structure as the signal beam (E_T) (see Eq. (4)). This result is illustrated by Figure 3b, where E_D is displayed with the same shape as E_T on Figure 3a, but with a smaller amplitude ($\eta < 1$).

The signal (E_T) and diffracted (E_D) beams are thus spatially coherent. They can interfere constructively (or destructively) on a large-area ($\sim 1\,\mathrm{cm}^2$) light mono detector (*i.e.* a photodiode). This property will be useful to detect efficiently the tagged and untagged photons signal.

3.3 Detection of the tagged photons

The principle of tagged photons detection is illustrated by Figure 5. The phase φ of the US beam is reversed periodically ($\varphi = 0$ or π) with period T (see Fig. 5c). The phase of the tagged photons field E_T, which follows the US phase, is then reversed too.

To simplify the discussion, we will neglect the decorrelation of the tagged photons field (Eq. (5) is fulfilled). We will also modulate the phase rapidly (with respect to T_{PR}, *i.e.* with $T \ll T_{PR}$), keeping φ zero most of the time (see Fig. 5c), so that the hologram can be considered as static and unperturbed by the phase variation.

In that case, the diffracted field E_D will remain nearly constant: $E_D \simeq \eta \langle E_T \rangle$. When φ is zero, E_T and E_D are in phase, they interfere constructively and the total intensity signal $|E_T + E_D|^2$ is maximum (see Fig. 5a):

$$I_0 = (|E_T + E_D|^2)_{\varphi=0} \simeq |E_T|^2 (1+\eta)^2. \tag{6}$$

On the contrary, when the phase is π, E_T and E_D are opposite in phase, and the total intensity signal is minimum (see Fig. 5b):

$$I_\pi = (|E_T + E_D|^2)_{\varphi=\pi} \simeq |E_T|^2 (1-\eta)^2. \tag{7}$$

Reversing the phase of the US yields a modulation of the total intensity signal equal to

$$I_0 - I_\pi \simeq 4\eta|E_T|^2 + \dots . \tag{8}$$

3.4 Detection of the untagged photons

It is a little bit more difficult to illustrate the detection of the untagged photons with a simple figure, because the calculation involves considering both the untagged photons field at the carrier frequency ω_L, and the tagged photons fields E_T and $E_{T'}$, which evolves at the two sideband frequencies $\omega_L + \omega_A$ for E_T, and $\omega_L - \omega_A$ for $E_{T'}$. To detect the untagged photons, we tune the reference beam frequency ω_R at the untagged photons frequency, $\omega_R = \omega_L$, and we modulate the US beam intensity by turning on and off the US beam.

To simplify the discussion, we will neglect again the decorrelation of the tagged photons field (Eq. (5) is fulfilled). We will also modulate the US beam rapidly (with respect to T_{PR}, *i.e.* with a period $T \ll T_{PR}$). Let us call E_U and $E_{U'}$ the untagged photons fields without, and with the US beam. E_T and $E_{T'}$ are the tagged photons fields with US (theses fields are zero without US).

Since the energy is conserved, the total number of photons (carrier + sidebands) does not depend on the US. We get thus

$$|E_U|^2 = |E_{U'}|^2 + |E_T|^2 + |E_{T'}|^2. \tag{9}$$

The untagged photons field in the presence of US, *e.g.*, $E_{U'}$, is spatially coherent with the one without US, *e.g.*, E_U. According to equation (9), its magnitude can be expressed as follows:

$$|E_{U'}| = |E_U|\sqrt{1 - \frac{|E_T|^2 + |E_{T'}|^2}{|E_U|^2}}\,. \tag{10}$$

In practical situations, the efficiency of the acousto-optic effect is low and the energy within the sideband is low ($< 1\%$) with respect to the carrier. This means that the untagged photons field variation is low: $E_U - E_{U'} \ll E_U$. Whatever the value of the cyclic ratio modulation is, one can thus consider that the PR effect involves E_U only. We get

$$E_D \simeq \eta E_U. \tag{11}$$

When the US is off, the field on the detector is $E_U + E_D$ and the detected intensity signal I is

$$I = |E_U + E_D|^2 \tag{12}$$
$$= |E_U|^2 + |E_D|^2 + 2\eta|E_U|^2. \tag{13}$$

When the US is on, the field on the detector is $E_{U'} + E_D$ for the carrier, and E_T and $E_{T'}$ for the two sidebands. The intensity signal I' is

$$I' = |E_{U'} + E_D|^2 + |E_T|^2 + |E_{T'}|^2 \tag{14}$$
$$= |E_{U'}|^2 + |E_D|^2 + \eta(E_{U'}E_U^* + E_U E_{U'}^*) + |E_T|^2 + |E_{T'}|^2. \tag{15}$$

Taking into account the energy conservation (Eq. (9)), the spatial coherence of (E_U, $E_{U'}$) and Eq. (10), we get the modulation of the detected intensity

$$I - I' = 2\eta(|E_U|^2 - |E_{U'}| \cdot |E_U|) \tag{16}$$
$$\simeq 2\eta\frac{|E_T|^2 + |E_{T'}|^2}{2} \simeq 2\eta|E_T|^2, \tag{17}$$

since the weight of the two sidebands components is approximately the same: $|E_T|^2 \simeq |E_{T'}|^2$.

By comparing equation (8) and equation (16), the detected signals have the same order of magnitude when detecting either the tagged or the untagged photons, when we consider the same acoustical energy.

3.5 Detecting tagged or untagged photons?

To our knowledge, three groups are working on acousto-optic imaging with PR detection of the signal. Two of them, the R.A. Roy [17, 21–23] and the L.V. Wang group [24] detect the untagged photons. We are the third group [16,25] and we detect both the tagged and untagged photons.

Detection of the untagged photons is simpler, since it is not necessary to shift the frequency the reference beam ($\omega_R = \omega_L$). The acousto-optic modulators of Figure 4 are thus not needed. Moreover, it is not necessary to apply the US beam all the time. Untagged photons detection is thus well suited to detect very short burst of US beam able to give information resolved along the US beam propagation direction [17]. But short US bursts yield a small signal, and the signal is needed to image thick breast *in vivo*.

The detection of the untagged photons corresponds to a small change on a large signal (white background detection), while the detection of the tagged photons, which corresponds to roughly the same absolute value change, yields on the contrary about 100% change on a small signal (black background detection). Tagged photon detection is thus expected to give less technical noise. For example, vibrations on the reference beam mirrors, which modify the length of the pump beam arm, are expected to yield about 100 times[2] more noise for the untagged configuration than for the tagged one.

The tagged photon configuration offers more degrees of freedom for the detection configuration, because the signal and the reference beam can be modulated whether in phase or amplitude.

Since we do not have tested all the possible detection configurations, making a complete comparison of tagged and untagged photons detection schemes is out of the scope of the present paper. We can simply say that for the configurations we have presently tested, the Signal-to-Noise Ratio (SNR) is about the same in the two cases. Since our purpose is to image breast, we need to improve the detection sensitivity. We continue thus to work with our setup that is able to detect both tagged and untagged photons, exploring configurations that are expected to yield better SNR. This work is under progress.

[2] Here 100 is the untagged *versus* tagged photons field ratio.

4 Experimental test

4.1 Setup

A typical experimental setup, able to select either the tagged or the untagged photons, is shown in Figure 6. The main laser beam is splitted in an illumination and reference beam by the beam splitter BS. The US beam (2 MHz) produced by the generator PZT is focused within the sample. The frequency offset of the illumination beam is adjusted by using the two acousto-optic modulators AOM1 and AOM2 which are excited at 78 MHz and 76 MHz (for selecting the tagged photons), or both at 78 MHz (for selecting the untagged photons). The light diffused by the sample is collected by the high N.A. ~ 1 (Numerical Aperture) lenses L1 and L2. L1 collects the light within the PR crystal that records the hologram of the selected signal beam (tagged or untagged). L2 collects the interference pattern of the signal beam (E_T) with the diffracted beam (E_D) into the photodetector PD.

In our setup, L is a Nd:YAG laser (1.06 μm, 1 to 5 W CW power), the PR crystal is a $1.4 \times 1.4 \times 2\,\mathrm{cm}^3$ GaAs crystal [26], and PD is a large-area photodiode (0.1 to $0.5\,\mathrm{cm}^2$) whose signal is amplified by a transimpedance amplifier ($R = 100\,\mathrm{K}\Omega$ to $10\,\mathrm{M}\Omega$).

In Murray's setup [17], L is a frequency-doubled Nd:YAG (532 nm, 80 mW), the PR crystal is a $5 \times 5 \times 7\,\mathrm{mm}^3$ $Bi_{12}SiO_{20}$ crystal, whose PR efficiency is improved by applying a DC electric field, the US frequency is 1.1 MHz, and PD is an avalanche photodiode. Since Murray detects the untagged photons, the acousto-optic modulators are not present, but it should be pointed out that absorption at 532 nm is more important than at 1064 nm, and thus it can reduce the thickness of investigation.

Our setup, which can detect both the tagged and untagged photons, is expected to be more sensitive, while Murray's setup, which is used with short US pulses, is faster.

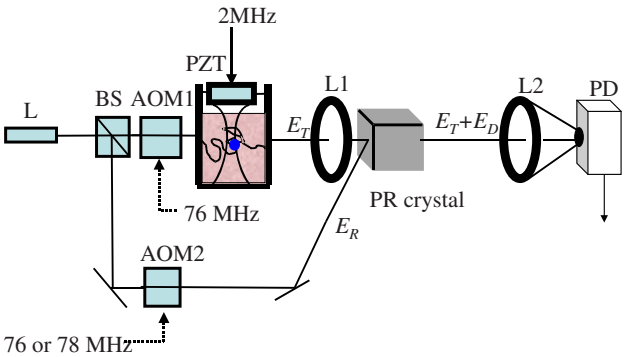

Fig. 6. Typical experimental setup. L: laser; BS: beam splitter; AOM1, AOM2: acousto-optic modulators; PZT: US generator; L1, L2: light-collecting lenses; PR: photorefractive crystal; PD: photodetector.

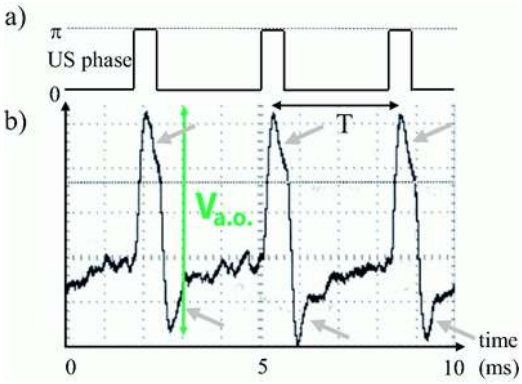

Fig. 7. Typical tagged photons experimental signal. a) Modulation of the US phase. b) Tagged photons signal. $V_{\mathrm{a.o.}}$: maximum variation of the tagged photons signal. T: phase modulation period. The vertical axis is the voltage at the output of the PD amplifier: 100 mV per div.

4.2 Experimental result

Figure 7 shows a typical tagged photons experimental signal obtained with 0 to π phase modulation of the US beam. The modulation frequency is 300 Hz (modulation period $T = 3.33$ ms). The US beam frequency is 2 MHz, with a maximum US pressure of 2 MPa at the US beam waist. The main laser power is 1.2 W. The reference and illumination beam power are both 300 mW, their areas on crystal and sample are both $1\,\mathrm{cm}^2$.

Measurement is performed with a 4 cm chicken sample, whose optical properties (diffusion and absorption) are close to human breast. As seen, the tagged photons signal SNR is good (16 times averaged). One must notice that the signal is not rectangular like the phase modulation. In particular, the maximum of the signal, which occurs on the phase plateaus ($\varphi = \pi$ and 0) is not flat, but decreases exponentially (see grey arrows in Fig. 7).

This is expected when the PR time T_{PR} becomes shorter than the phase modulation period T. We have measured (see further) T_{PR} and we have found $T_{PR} = 0.5$ ms. Note that T_{PR} can also be measured in Figure 7, since T_{PR} is the time constant of the grey arrow decay.

This result is very encouraging, because it means that the detection bandwidth is $1/(2\pi T_{PR}) = 0.3$ kHz. Remember that the signal bandwidth is $\Delta\omega = 1.5$ kHz (HWHM) on the breast. The detection is thus optimal, within a factor 5. Since the SNR is very high (much larger than 5) in Figure 7, we expect to get enough SNR to get significant result with a thick living sample.

As another illustration, Figure 8(a) represents a profile of an Agar plus *Intralipid* phantom with a thickness $t = 30$ mm and a reduced scattering coefficient $\mu_s' = 1/l_s^* = 10\,\mathrm{cm}^{-1}$ at 1064 nm. The absorption coefficient of water at 1064 nm is $\mu_a = 0.144\,\mathrm{cm}^{-1}$ [27]. The sample contains an optical absorber (black ink), which is a cylinder with a diameter of 3 mm and a height of 7 mm along the laser input direction (perpendicular to the US beam). The magnitude of the US pressure is approximately of 1.5 MPa at 2.3 MHz, with a phase modulation at 3 kHz and a duty cycle of 24%, corresponding to the maximum of the signal with a lock-in detection [16, 25]. The photorefractive

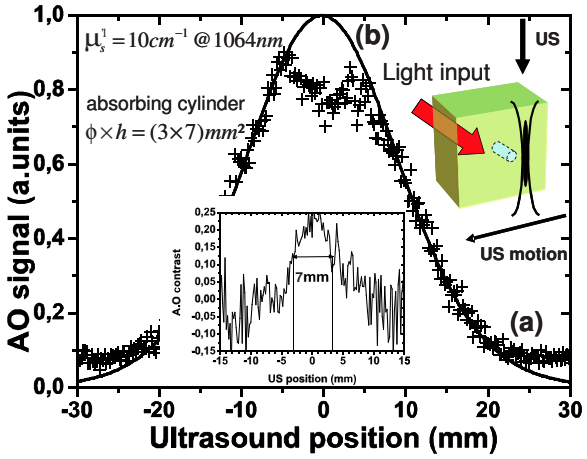

Fig. 8. Acousto-optic profile (a) with an optical absorber embedded within an Agar + *Intralipid* phantom of thickness $t = 30\,\text{mm}$ with a reduced scatttering coefficient $\mu_s' = 10\,\text{cm}^{-1}$ at 1064 nm obtained with an anisotropic (PR) detection configuration. Light input on the sample is $1\,\text{W/cm}^2$ (Gaussian illumination FWHM = 1.1 mm). The US pressure (2.3 MHz, 1.5 MPa) is phase modulated at 3 kHz with a duty cycle of 24%. Curve (b) represents a fit of the one-dimensional extent of light scattering (*i.e.* $\exp(-\mu_{eff}r)/r$, with $\mu_{eff} = 2.2\,\text{cm}^{-1}$) within the US plane (15 mm from input window), weighted by the input illumination $\mu_{eff} = 2.2\,\text{cm}^{-1}$. The inset represents the acousto-optic contrast $[1-(a)/(b)]$.

holographic setup is based on an anisotropic diffraction configuration [28]: the reference beam (*i.e.*, vertically polarized) diffracts a contribution (*i.e.*, tagged-photons field) which is perpendicularly polarized (*i.e.*, horizontal); the output speckle from the sample is 45°-polarized from the vertical direction using a large-aperture infrared dichroic polarizer, and a similar analyzer is positioned in front of the photodetector with a horizontal polarization axis. Consequently, the speckle and the reference fields still interfere within the PR crystal in order to build the hologram, the diffracted reference and the speckle field recombine onto the analyzer as well. This configuration minimizes the collection of the unwanted scattered reference by the PR crystal faces. In this experiment the tagged light is about $\times 10^4$ lower than the total scattered light (untagged photons plus scattered reference light).

Classically, in the $3D$ diffusion regime and in the presence of absorption, the spatial distribution of the energy emitted from a point source at distance r is given by $\frac{1}{r}e^{-\mu_{eff}r}$, where $\mu_{eff} = \sqrt{3\mu_a(\mu_a+\mu_s')}$. This effective parameter indicates that attenuation is increased by scattering, that lengthens optical paths.

The continuous envelope Figure 8(b) represents the fit the experimental data of Figure 8(a) using this model and taking into account the Gaussian input illumination (FWHM = 1.1 mm). The effective coefficient μ_{eff} is found to be $2.2\,\text{cm}^{-1}$, close to the theoretical value ($\mu_{eff} = 2.1\,\text{cm}^{-1}$) given by the reduced scattering coefficient of the medium and the absorption coefficient of pure water at 1064 nm defined above. The measured background (around 0.8 mV) corresponds to the noise of the transimpedance stage of the detection, that is shot-noise–limited at this level of the scattered light. The absorbing element is revealed by the acousto-optic contrast, *e.g.* $[1-(a)/(b)]$, which is close to 0.22, and exhibits a FWHM of 7 mm. This value is connected to the diameter of the absorbing element (3 mm), the US resolution (just above 1.5 mm) and the light transport mean free path l_s^* of the scattering medium (about 1 mm).

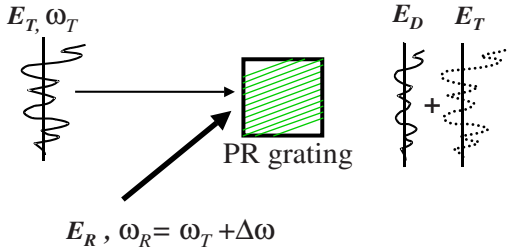

Fig. 9. PR effect when the selected photons and reference beam frequencies are different: $\omega_R \neq \omega_T$.

5 Measurement of the photorefractive time T_{PR}

Most published results on ultrasound light modulation imaging have been obtained with phantoms, which do not decorrelate in time. In that case, the PR detection SNR does not strongly depend on the reference beam power. The power must be large enough to reach the plateau value for the photorefractive efficiency η, but remains low enough to avoid noise (the reference beam is scattered by the PR crystal defects yielding a parasitic photodiode current that brings noise). With phantoms, the best sensitivity is then obtained with a quite low power reference beam (< 100 mW in our experiment).

With breast, the light signal is Doppler broadened by the tissues inner motions (Brownian motion, blood flow, ...) yielding typically a spectral width of 3 kHz [4]. In order to optimize the detection efficiency, one must increase the detection bandwidth $1/T_{PR}$ by increasing the reference beam power to obtain $1/T_{PR} \sim 3\,\text{kHz}$. Optimal detection conditions for phantoms and breast are thus very different.

To improve the detection sensitivity for future breast experiment, it is very important to measure T_{PR}. To get a reliable result, we have proposed a technique able to measure T_{PR} *in situ*, *i.e.* in the setup that is used for imaging phantoms (and breast in the future) [29].

5.1 Principle of the measurement of T_{PR}

To perform acousto-optic imaging with living sample, it is very important to measure T_{PR}, since it is necessary to match T_{PR} with the sample decorrelation time in order to optimize the detection efficiency. The ability in our setup to freely choose the frequency of the reference beam gives new opportunity to measure the photorefractive time T_{PR}.

The idea of the measurement technique is illustrated by Figure 9. The frequency of the reference beam ω_R is

shifted with respect to the signal beam frequency $\omega_T = \omega_L + \omega_A$ or ω_L

$$\omega_R = \omega_T + \Delta\omega. \tag{18}$$

To simplify the notation, we will consider that E_R still represents a complex field projection at frequency ω_T, so that E_R must be replaced in the calculation with $E_R\, e^{j\Delta\omega t}$. We get thus

$$\delta n(t) \propto \frac{\langle E_T E_R^*\, e^{-j\Delta\omega t}\rangle_{T_{PR}}}{|E_T|^2 + |E_R|^2} \tag{19}$$

and

$$E_D(t) \propto \frac{E_R\, e^{j\Delta\omega t}}{T_{PR}} \frac{\displaystyle\int_0^\infty E_T(t-\tau) E_R^*\, e^{-j\Delta\omega\tau}\, e^{-\tau/T_{PR}} \mathrm{d}\tau}{|E_T|^2 + |E_R|^2}. \tag{20}$$

Note that if $\Delta\omega$ is zero, equation (20) is identical to equation (3). Note also that E_R^* does not depend on time, and can thus be removed from the integral.

Consider that a PR experiment is made with a sample whose decorrelation time is much longer than T_{PR}. This means that decorrelation can be neglected, and that $E_T(t)$ is uniquely driven by the US amplitude or phase modulation. $E_T(t)$ is thus known. $|E_T|^2$ can also be neglected in the denominator of equation (20) (since $|E_T|^2 \ll |E_R|^2$) and thus

$$E_D(t) \propto \frac{e^{j\Delta\omega t}}{T_{PR}} \int_0^\infty E_T(t-\tau) e^{-j\Delta\omega\tau}\, e^{-\tau/T_{PR}}\, \mathrm{d}\tau\, e^{j\Delta\omega t}. \tag{21}$$

We must notice that in equation (21), $E_T(t)$ is convolved by two time kernels. The first kernel $e^{-\tau/T_{PR}}$ is unknown (since T_{PR} is unknown), while the second $e^{-j\Delta\omega\tau}$ is known. Its width can be freely adjusted by tuning $\Delta\omega$ with the acousto-optic modulator.

From equation (20) it is then straightforward to calculate the dependence of the acousto-optic signal on $\Delta\omega$ for the different detection configurations (phase modulation for the tagged photons and amplitude modulation for the untagged photons) [29]. Comparing the calculated spectrum to the experiment yields then an accurate measurement of T_{PR}.

5.2 Calculation of the tagged photons signal with US amplitude modulation

It is possible to calculate the tagged photons signal as a function of $\Delta\omega$ in the phase modulation configuration. Nevertheless, as shown in [29], the shape of the spectrum is quite cumbersome, and it seems quite heavy to fit the experimental data with such a spectrum shape.

It is thus more efficient to measure T_{PR} with a rectangular amplitude modulation of the US with 50% cycling ratio, the tagged (or untagged) acousto-optic signal being measured with a lock-in amplifier tuned at the modulation frequency. This is the key point of the detuning method, since measurements are performed *in situ* at the US modulation frequency (here 2.5 kHz) and thus do not depend on the frequency response of the detector, which is quite distorted due to the many stages of the electronic filters connected to the photodetector. A straightforward calculation gives only three contributions for the P and Q quadrature of the lock-in signal [29]

$$P = P_0 + P_+ + P_-, \tag{22}$$

$$Q = Q_0 + Q_+ + Q_-, \tag{23}$$

with

$$P_0(\Delta\omega) = \frac{2A}{1 + (\Delta\omega T_{PR})^2}, \tag{24}$$

$$P_\pm(\Delta\omega) = \frac{A}{1 + (\omega_{mod} \mp \Delta\omega)^2\, T_{PR}^2}, \tag{25}$$

$$Q_\pm(\Delta\omega) = -\frac{A(\omega_{mod} \mp \Delta\omega) T_{PR}}{1 + (\omega_{mod} \mp \Delta\omega)^2\, T_{PR}^2}, \tag{26}$$

where A is a proportional constant. By using equation (24) to equation (26) it is then quite simple to measure T_{PR} by fitting the experimental data with the calculated $\Delta\omega$ spectrum.

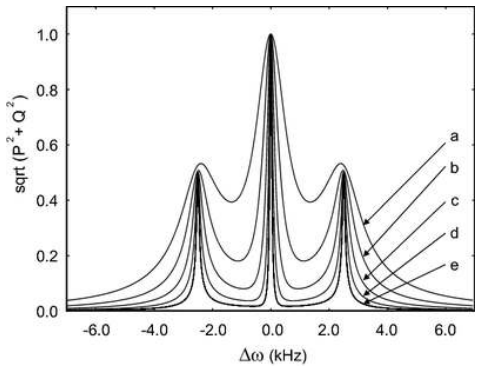

Fig. 10. Calculated spectrum of the tagged photons signal (amplitude modulation with 50% cycling ratio) with T_{PR} = 0.25 ms (a), 0.5 ms, (b), 1 ms (c), 2 ms (d), 4 ms (e). The horizontal axis is the frequency offset $\Delta\omega$. The vertical axis is the $\sqrt{P^2 + Q^2}$ lock-in signal in arbitrary normalized units.

5.3 Measurement with the tagged photons and US amplitude modulation

From equation (22) to equation (26) we have calculated the tagged photons signal as a function of $\Delta\omega$, when the US beam is modulated with a rectangular $[0, 1]$ amplitude modulation of 50% cycling ratio, the detection being performed with a lock amplifier tuned at the modulation frequency (2.5 kHz). As seen in Figure 10 the shape of the spectrum is strongly dependent on T_{PR}.

It is then possible to fit experimental data on the theoretical curves. Figure 11 shows the magnitude (*i.e.* $R = \sqrt{P^2 + Q^2}$) of the lock-in signal (points). The tagged photons are selected ($\omega_R = \omega_L + \Delta\omega$) and the US beam is modulated in amplitude with 50% duty cycle. The reference beam flux is 300 mW/cm^2, and the modulation frequency is 2.5 kHz. We have fitted the experimental data with the theoretical curve deduced from equation (24) to

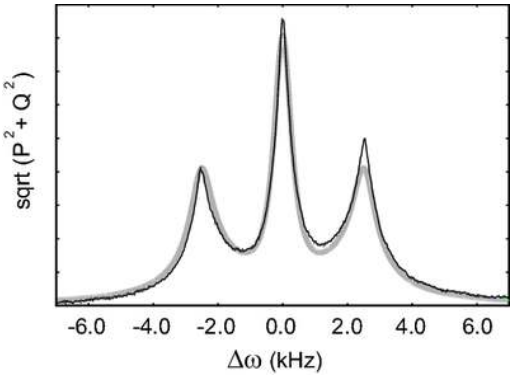

Fig. 11. Spectrum of the tagged photons signal with 50% duty cycle amplitude modulation of the US. The black curve is the experimental data with a reference beam flux of 300 mW/cm^2 and a modulation frequency of 2.5 kHz. The heavy grey line curve is the calculated spectrum with $T_{PR} = 0.45$ ms. The horizontal axis is the frequency offset $\Delta\omega$. The vertical axis is the $\sqrt{P^2 + Q^2}$ lock-in signal in arbitrary units.

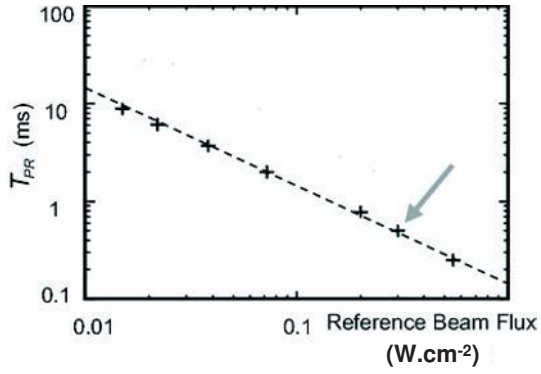

Fig. 12. T_{PR} in ms as a function of the reference beam flux in W/cm^2. Crosses are experimental data. The dashed line is data extrapolation with slope -1. The grey arrow corresponds to Figure 7 experimental conditions.

equation (26). The fit free parameters are T_{PR} and A. The best fit yields $T_{PR} = 0.45$ ms. The experimental data are shown in Figure 11 as a black curve, the fit as a heavy-grey-line curve.

We have recorded many spectra for different reference beam flux. Each spectrum has been fitted by the theoretical curve yielding T_{PR}. Figure 12 shows T_{PR} as a function of the reference beam flux in a logarithmic scale. Experimental points are crosses, data linear log-log extrapolation is the dashed line. As seen, the slope of the extrapolation line is -1. This means that T_{PR} is inversely proportional to the beam flux, as expected.

The shortest photorefractive time we get is $T_{PR} = 0.25$ ms for a flux of 0.55 W/cm^2. The Figure 7 modulation phase signal is obtained with $T_{PR} = 0.5$ ms and 0.3 W/cm^2 (grey arrows in Fig. 7).

6 Conclusion

Seeing through highly scattering media such as living tissues is a goal difficult to reach. Coupling light and ultrasound in acousto-optic imaging is a promising method to reach this aim. Nevertheless the efficient detection of the tagged photons remains a challenge.

The PR crystal detection scheme proposed here is a possible way to solve this problem. PR crystal detection has many advantages. The detection optical *etendue* is large since the photodetector area may be quite large (~ 1 cm^2), and since the collecting lens numerical aperture can be large, too (NA ~ 1). Since the detector is a single-detector (photodiode), the analysis of the data is simple and fast. By adjusting the power of the pump beam, it is possible to match the detection bandwidth $1/T_{PR}$ with the signal bandwidth $\Delta\omega$ in order to detect with optimal efficiency the "tagged" or "untagged" signal diffused by living tissues that are broadened by the diffuser inner motion (Brownian motion, blood flow, ...). We demonstrate here our ability to get a high SNR (see Fig. 7) with a thick chicken sample. Our chicken sample does not decorrelate as do living tissues, the measurement is done with a short photorefractive time $T_{PR} = 0.5$ ms. This result is very encouraging.

The results presented in this paper have been obtained with a Nd:YAG laser at 1064 nm and a GaAs photorefractive crystal. The method could be significantly enhanced by the use of a laser source at 800 nm, according to the absorption coefficients of hemoglobin and de-oxyhemoglobin, in order to perform a measurement of the local blood activity (two wavelengths measurements). We are searching at present for new PR crystals that are sensitive in this spectral range.

This work is currently supported by a grant from the project Cancéropôle Ile-de-France.

References

1. W. Leutz, G. Maret, Physica B **204**, 14 (1995).
2. L.H. Wang, S.L. Jacques, X. Zhao, Opt. Lett. **20**, 629 (1995).
3. M. Kempe, M. Larionov, D. Zaslavsky, A.Z. Genack, J. Opt. Soc. Am. **14**, 1151 (1997).
4. M. Gross, P. Goy, B.C. Forget, M. Atlan, F. Ramaz, A.C. Boccara, A.K. Dunn, Opt. Lett. **30**, 1357 (2005).
5. A. Lev, B.G. Sfez, J. Opt. Soc. Am. A **20**, 2347 (2003).
6. F.A. Marks, H.W. Tomlinson, G.W. Brooksby, in *Photon Migration and Imaging in Random Media and Tissue*, edited by B. Chance, R.R. Alfano, *Proc. SPIE*, Vol. **1888** (1993) pp. 500–510.
7. L. Wang, S.L. Jacques, L. Zheng, Comput. Methods Programs Biomed. **47**, 131 (1995).
8. A. Lev, Z. Kotler, B.G. Sfez, Opt. Lett. **25**, 378 (2000).
9. L.H. Wang, Q. Shen, Opt. Lett. **23**, 561 (1998).
10. A. Lev, B.G. Sfez, Opt. Lett. **27**, 473 (2002).
11. S. Lévêque, A.C. Boccara, M. Lebec, H. Saint-Jalmes, Opt. Lett. **24**, 181 (1999).
12. S. Lévêque-Fort, Appl. Opt. **40**, 1029 (2000).
13. S. Lévêque-Fort, J. Selb, L. Pottier, A.C. Boccara, Opt. Commun. **196**, 127 (2001).
14. M. Gross, P. Goy, M. Al-Koussa, Opt. Lett. **28**, 2482 (2003).

15. M. Atlan, B.C. Forget, F. Ramaz, A.C. Boccara, M. Gross, Opt. Lett. **30**, 1360 (2005).
16. F. Ramaz, B.C. Forget, M. Atlan, A.C. Boccara, M. Gross, P. Delaye, G. Roosen, Opt. Express **29**, 5469 (2004).
17. T.W. Murray, L. Sui, G. Maguluri, R.A. Roy, A. Nieva, F. Blonigen, C.A. DiMarzio, Opt. Lett. **12**, 2509 (2004).
18. A. Yariv, *Quantum Electronics*, third edition (John Wiley and Sons Inc., 1989) pp. 516–529.
19. Ph. Delaye, L.A. de Montmorillon, G. Roosen, Opt. Commun. **118**, 154 (1995).
20. L.A. de Montmorillon, Ph. Delaye, J.C. Launay, G. Roosen, J. Appl. Phys. **82**, 5913 (1997).
21. E. Bossy, T.W. Murray, L. Sui, R.A. Roy, Opt. Lett. **30**, 744 (2005).
22. C. DiMarzio, L. Sui, R.A. Roy, T.W. Murray, Appl. Opt. **44**, 4041 (2005).
23. C. DiMarzio, S. Manneville, L. Sui, G. Maguluri, T.W. Murray, F.J. Blonigen, A. Nieva, R.A. Roy, Appl. Opt. **44**, 3735 (2005).
24. J. Li, S. Sakadzic, G. Ku, L.V. Wang, Appl. Opt. **42**, 4088 (2003).
25. M. Gross, F. Ramaz, B.C. Forget, M. Atlan, A.C. Boccara, P. Delaye, G. Roosen, Opt. Express **13**, 7097 (2005).
26. P. Delaye, L.A. de Montmorillon, H.J. von Bardeleben, G. Roosen, Appl. Phys. Lett. **64**, 2640 (1994).
27. Linhong Kou, Daniel Labrie, Petr Chylek, Appl. Opt. **32**, 3531 (1993).
28. T.Y. Chang, A.E. Chiou, P. Yeh, J. Opt. Soc. Am. B **5**, 1724 (1988).
29. M. Lesaffre, F. Jean, F. Ramaz, A.C. Boccara, M. Gross, P. Delaye, G. Roosen, Opt. Express **15**, 1030 (2007).